J|A|C|S
ARTICLES
Published on Web 07/19/2003

A New Angle on Heat Capacity Changes in Hydrophobic Solvation

Kelly R. Gallagher and Kim A. Sharp*

Contribution from the Johnson Research Foundation and Department of Biochemistry and Biophysics, University of Pennsylvania, Philadelphia, Pennsylvania 19104

Received December 18, 2002; E-mail: sharpk@mail.med.upenn.edu

Abstract: The differential solubility of polar and apolar groups in water is important for the self-assembly of globular proteins, lipid membranes, nucleic acids, and other specific biological structures through hydrophobic and hydrophilic effects. The increase in water's heat capacity upon hydration of apolar compounds is one signature of the hydrophobic effect and differentiates it from the hydration of polar compounds, which cause a decrease in heat capacity. Water structuring around apolar and polar groups is an important factor in their differential solubility and heat capacity effects. Here, it is shown that joint radial/angular distribution functions of water obtained from simulations reveal quite different hydration structures around polar and apolar groups: polar and apolar groups have a deficit or excess, respectively, of "low angle hydrogen bonds". Low angle hydrogen bonds have a larger energy fluctuation than high angle bonds, and analysis of these differences provides a physical reason for the opposite changes in heat capacity and new insight into water structure around solutes and the hydrophobic effect.

Introduction

The differential solubility of polar and apolar groups in water is crucial for the self-assembly of globular proteins, lipid membranes, nucleic acids, and other specific biological structures through the hydrophobic effect (the attraction between apolar groups in aqueous solution) and its converse, the hydrophilic effect (the attraction of polar groups to water). Early studies of the hydrophobic effect focused on the unfavorable decrease in water entropy caused by apolar groups.[1,2] Subsequent important but puzzling experimental results demonstrated that a solute's effect on water's heat capacity (C_p), rather than its entropy, is a better key to understanding hydrophobic solvation and its contribution to protein stability.[3−5] C_p describes the dependence of the three major thermodynamic parameters, entropy (S), enthalpy (H), and Gibbs free energy (G), on temperature (T) by:

$$C_p = T\,\mathrm{d}S/\mathrm{d}T = \mathrm{d}H/\mathrm{d}T = -T(\mathrm{d}^2G/\mathrm{d}T^2) = \delta H^2/kT^2 \quad (1)$$

respectively, where δH^2 is the mean squared fluctuation in enthalpy. The hydration heat capacity (ΔC_p) of apolar groups is positive,[4−6] which, by the first equality in eq 1, means that their hydration entropy (ΔS) becomes less negative with temperature and becomes positive around 110 °C, and yet the phenomenon of hydrophobicity persists, and some hyperthermophilic proteins can remain stable above this temperature. Second, because the exposure of hydrophobic groups to water imparts a net positive ΔC_p of unfolding for many proteins, by the third equality of eq 1, the stability ($\Delta G^{\mathrm{unfold}}$) has a downward curvature as a function of temperature. This means that the stability of a protein will be a maximum at some temperature and is decreased both by raising and by lowering the temperature. The latter consequence of the C_p change, which results in an increase in the solubility of apolar groups in water at lower temperatures, is responsible for the phenomenon of cold denaturation.[4] Finally, only ΔC_p differentiates by sign between apolar solutes (positive) and polar solutes (negative), whereas ΔS and ΔH for apolar and polar solutes are both negative at physiological temperature.[7−9] Although the entropy decrease indicates that water is structured around both polar and apolar groups, clearly the structuring is different.

Specific information about water structure is provided almost entirely by scattering experiments, which directly measure radial distribution functions ($g(r)$, the probability distribution for the separation of pairs of atoms). The complete set of $g(r)$'s for water (between O−O, H−H, and OH) have been measured.[10−13] Consequently, the radial structure of pure water is well characterized. Yet experimentally determined $g(r)$'s change rather little in the presence of hydrophobic solutes,[10,13] for a number of reasons, including incomplete mixing of the solute, the masking contribution of bulk water (i.e., that not in the

(1) Kauzmann, W. *Adv. Protein Chem.* **1959**, *14*, 1−63.
(2) Tanford, C. H. *The Hydrophobic Effect*; John Wiley and Sons: New York, 1980.
(3) Kauzmann, W. *Nature* **1987**, *325*, 763−4.
(4) Privalov, P. L.; Gill, S. J. *Adv. Protein Chem.* **1988**, *39*, 191−234.
(5) Murphy, K. P.; Privalov, P. L.; Gill, S. J. *Science* **1990**, *247*, 559−561.
(6) Baldwin, R. *Proc. Natl. Acad. Sci. U.S.A.* **1986**, *83*, 8069−8072.
(7) Cabani, S.; Gianni, P.; Mollica, V.; Lepori, L. *J. Solution Chem.* **1981**, *10*, 563−595.
(8) Ben-Naim, A.; Marcus, Y. *J. Chem. Phys.* **1984**, *81*, 2016−2027.
(9) Marcus, Y. *Biophys. Chem.* **1994**, *51*, 111−128.
(10) Turner, J.; Soper, A. *J. Chem. Phys.* **1994**, *101*, 6116−6125.
(11) Turner, J.; Soper, A.; Finney, J. *J. Chem. Phys.* **1995**, *102*, 5438−5443.
(12) Soper, A. K. *Chem. Phys.* **2002**, *258*, 121−37.
(13) Dixit, S.; Crain, J.; Poon, W.; Finney, J. L.; Soper, A. C. *Nature* **2002**, *416*, 829−32.

solute's first hydration shell), and the inherent insensitivity of radial distributions to the type of angular structure changes induced by solutes in water.[14] Water is notable among solvents for its large amount of angular structure, evinced, for example, by its low coordination number and the density increase upon melting. Partial angular structure information has been reconstructed by maximum entropy methods from the $g(r)$'s of pure water.[15,16] This study, and simulations of water's orientational structure,[17] provide a very similar picture of the first coordination shell of water: Water clusters quite tightly in the tetrahedral positions along the two O−H (H-bond donor) directions, but there is a broader band of density spread between the other two tetrahedral, or two "lone-pair", positions around the O (the H-bond acceptor directions). Although a partial orientational analysis of water around the "hydrophobic" ion tetramethylammonium (TMA) confirms that the hydrating water structure is "apolar-like",[11] experimental studies of angular water structure around polar and apolar solutes at this level of detail for comparison are unfortunately not available. Computer simulations have thus been used extensively to study solvation. With regard to the angular aspect, studies of the H-bonding geometry with respect to hydrophobic solutes and surfaces have been made,[18−21] and the effect of solute shape and polarity on the orientation of water at the solute surface has been studied in detail;[22] see Pratt and Pohorille for a comprehensive review.[23] How these structural changes are reflected in hydration heat capacities of solutes and how they might explain the differential effect of polar and apolar groups is not known. A significant problem in this area is the reliable extraction of C_p from solute/water simulations. Examination of eq 1 shows that even the most practical approach, via the temperature derivative of the enthalpy, requires taking the difference between a minimum of two simulations, and evaluation of the hydration heat capacity requires the difference of this difference between pure water and water plus solute. Such a "brute-force" approach requires very long simulations and is practical only for the smallest and simplest apolar solutes. Even here, precision problems make obtaining the sign and magnitude of C_p changes a challenge.[24−27]

We have previously approached this problem by relating water structure changes around polar and apolar solutes to hydration heat capacities using an equation of state for C_p derived from the random network model (RNM) of water.[14,24,28−33] The approach clearly demonstrates the primary effect of angular structure changes, and it provides quantitative agreement with measured hydration C_p changes. However, the RNM parameters are obtained from fitting to data on pure water and ice, and their temperature dependencies are also obtained.[34] While this is satisfactory from a quantitative perspective, it does not explain why, in a physically interpretable way, a particular structural perturbation has the effect on C_p that it does.

To this end, we describe here a new analysis of water structure around both polar and apolar solutes that combines radial and angular distribution information, using water structure information obtained from extensive computer simulations of a wide range of solutes. We show that the analysis provides a rather simple physical explanation of the different effects of polar and apolar solutes upon water structure and provides a quantitative explanation of the heat capacity data.

Table 1. Solute First Hydration Shell Pairs

solute	ΔN	N_t	N_I	N_{II}
water	0.0	13.9	3.8	10.1
Ar	5.6	46.4	18.1	28.3
KI	−3.5	26.6	3.6	23.0
CsI	−2.5	28.0	5.0	23.0
CaI_2	−8.8	50.3	4.6	45.7
TMAI[a]	4.2	141.4	42.4	99.0
ethanol	8.0 (10.0,−2.0)[b]	78.4 (76.1,2.3)[b]	29.2	49.2
NMA[a]	9.5 (10.1,−0.6)[b]	102.9 (69.3,33.6)[b]	37.3	65.7
benzene	11.1	110.5	41.0	69.6
urea	3.6	58.9	19.5	39.4
TMAO	9.9	104.3	38.1	66.2
methane	7.0	53.5	21.4	32.1
ethane	8.8	81.4	30.8	50.6
propane	10.5	105.1	38.8	66.2
butane	11.5	110.1	41.2	68.9
cyclohexane	12.5	86.5	35.8	50.6
correlation with ΔC_p	$R = 0.97$	$R = 0.53$	$R = 0.79$	$R = 0.36$

[a] TMA: tetramethylammonium iodide. NMA: *N*-methylacetamide. [b] Figures in brackets are for the apolar and polar groups, respectively, of that solute.

Methods

The solvation of the solutes listed in Table 1 was simulated by inserting one copy of each of these molecules in turn into a box of water represented by the TIP4P potential.[35] Solutes were represented by the OPLS solute potential function[35,36] and included solute flexibility. For ionic solutes (KI, CsI, CaI_2, TMAI), the anion and cation were run as separate simulations, and then the resulting quantities were summed to give the neutral species values. The corresponding single ion experimental hydration C_p values were combined in the same way. This removes any uncertainty in the absolute value assumed for the H^+ ion in tabulating the experimental data as single ion quantities. The simulation method and its analysis have been described in detail in our earlier work.[14,28,29] A Metropolis Monte Carlo algorithm incorporated in the program BOSS[37] was used to run the simulations at constant temperature (298 K) and pressure (1 atm). Periodic boundary conditions and a nonbond cutoff of 12.0 Å were used. The pure water simulation and each of the solution simulations were first equilibrated for 5×10^7 Monte Carlo steps, and then data were collected over 10 consecutive runs of 10×10^7 steps each. The error estimates for the average quantities were computed from deviations of batch averages between the 10 runs. Simulations were performed with either 216 or 750 waters, with almost identical results on the structure of the first hydration shell, indicating a sufficiently large buffer of solvent. Distance−angle plots

(14) Madan, B.; Sharp, K. *Biophys. Chem.* **1999**, *78*, 33−41.
(15) Soper, A.; Ricci, M. *Phys. Rev. Lett.* **2000**, *84*, 2881−4.
(16) Soper, A. *J. Chem. Phys.* **1994**, *101*, 6888−6901.
(17) Svishchev, I.; Kusalik, P. *J. Chem. Phys.* **1993**, *99*, 3049−61.
(18) Lee, C. Y.; McCammon, J. A.; Rossky, P. J. *J. Chem. Phys.* **1984**, *80*, 4448.
(19) Lum, K.; Chandler, D.; Weeks, D. *J. Phys. Chem.* **1999**, *103*, 3, 4570−4577.
(20) Wilson, M.; Pohorile, A.; Pratt, L. *J. Phys. Chem.* **1987**, *91*, 4873−8.
(21) Lazaridis, T.; Paulaitis, M. *J. Phys. Chem.* **1994**, *98*, 635−42.
(22) Cheng, Y.-K.; Rossky, P. J. *Nature* **1998**, *392*, 696−699.
(23) Pratt, L.; Pohorille, A. *Chem. Rev.* **2002**, *102*, 2671−2692.
(24) Madan, B.; Sharp, K. A. *J. Phys. Chem.* **1996**, *100*, 7713−21.
(25) Swope, W. C.; Anderson, H. C. *J. Phys. Chem.* **1984**, *88*, 6548−6556.
(26) Arthur, J. W.; Haymet, A. D. J. *J. Chem. Phys.* **1999**, *110*, 5873−5883.
(27) Guillot, B.; Guissani, Y. *J. Chem. Phys.* **1993**, *99*, 8075−94.
(28) Sharp, K. A.; Madan, B. *J. Phys. Chem.* **1997**, *101*, 4343−48.
(29) Madan, B.; Sharp, K. A. *J. Phys. Chem.* **1997**, *101*, 11237−42.
(30) Vanzi, F.; Madan, B.; Sharp, K. *J. Am. Chem. Soc.* **1998**, *120*, 10748−53.
(31) Madan, B.; Sharp, K. A. *J. Phys. Chem.* **2000**, *104*, 12047−12047.
(32) Sharp, K.; Madan, B.; Manas, E.; Vanderkooi, J. *J. Chem. Phys.* **2001**, *114*, 1791−1796.
(33) Sharp, K. A.; Madan, B. *Biophys. J.* **2001**, *81*, 1881−1887.
(34) Henn, A. R.; Kauzmann, W. *J. Phys. Chem.* **1989**, *93*, 3770−3783.
(35) Jorgensen, W. L.; Chandrasekhar, J.; Madura, J. D.; Impey, R. W.; Klein, M. L. *J. Chem. Phys.* **1983**, *79*, 926.
(36) Jorgensen, W. L. *Chem. Phys. Lett.* **1982**, *92*, 405.
(37) Jorgensen, W. L. *BOSS, Version 3.3*; Copyright Yale University, New Haven, CT, 1992.

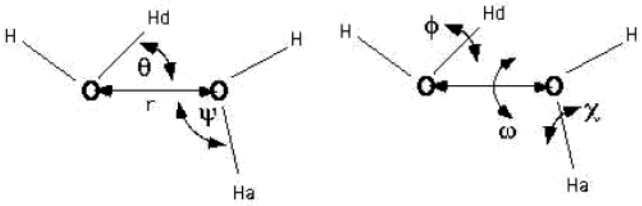

Figure 1. Definition of water pair separation and orientation. θ is the smallest of the four HO−O angles and defines the donor water and hydrogen (H_d), ψ is the smallest of the two HO−O angles on the acceptor water, ω is the dihedral angle formed by H^dO-OH_a, ϕ and χ are the orientations of the donor and acceptor waters around their HdO and OHa axes, respectively, with 0o defined when the second H lies in the HdO−O or O−OHa planes, respectively.

from the 216 water simulations are presented because the lower amount of noise reveals features more clearly.

A snapshot of the system was saved every 1000 Monte Carlo steps during each of the 10 data collection runs for subsequent analysis. In the first pass of analysis, solute atom−water oxygen radial distribution functions, $g_{xo}(r)$, were computed from the simulations, and the extent of the first and second hydration shell of each solute atom was determined from the position of the first and second minima of its $g_{xo}(r)$. In the second pass, all waters lying within a solute's first or second hydration shell were identified in each snapshot, on the basis of the solute−solvent $g_{xo}(r)$ minima, and, if necessary, each such water was further assigned to the hydration shell of the closest solute atom. After the partitioning of all of the water in each snapshot into the first shell, second shell, or bulk, the distance/angular configuration was computed for each pair of waters whose oxygens lay within 4.9 Å of each other. Pair configurations were binned by distance, angle, and shell (e.g., first−first, first−second...bulk−bulk), and normalized probability distributions were calculated. For multiatom solutes, first−first shell frequency distributions could be further subdivided on the basis of the solute atom pairs hydrated by the two waters as necessary; for example, for ethanol separate frequency distributions were calculated for first−first shell OH−OH and CH_3-CH_3 solvating water pairs. For NMA and other solutes containing both polar and apolar groups, waters were subdivided into polar hydrating and apolar hydrating.

The distance (r) and angle definitions used to analyze water pair geometries are shown in Figure 1. While our method of angular analysis is related to that used in previous work on pure water, there are some significant differences, primarily in the angular coordinate system we use and which components we focus on. In earlier work,[16,17] the two spherical polar angles were used to describe the position of one water with respect to another lying in the $x-z$ plane. Here, the primary angular coordinate, θ, is defined as the HO−O angle made by that hydrogen (designated here as the donor H_d) which makes the smallest angle (Figure 1a). This choice is motivated by several criteria. First, this is the definition used by Henn and Kauzmann[34] in developing their random network model, and it was shown in our previous studies of C_p to be a very sensitive marker for water structure changes.[14,38] Second, θ specifies, along with the O−O distance, the two strongest of the nine interwater atom−atom Coulomb interactions. Third, we find that, in situations where the two waters are H-bonded, defining the H-bond angle by θ is more sensitive, is independent of the O−O distance, and is more easily interpretable than the previous OH−O angle definition.[17,35]

To completely define the position/orientation of two waters, four other angles are needed in addition to r and θ. The ones used here are defined in Figure 1a. ψ is the smallest HO−O angle formed by the H on the acceptor water (H_a), ω is the dihedral angle formed by H_dO-OH_a, and ϕ and χ are the angles the other two OH bonds make with the H_dO-O and $O-OH_a$ planes, respectively. The distributions for these four angles were also computed from the simulations and analyzed, but they were found to either be rather insensitive to solute character or, in the case of ψ, reflect the same information as θ but in a less defined way (Supporting Information).

(38) Gallagher, K.; Sharp, K. A. *Biophys. Chem.* **2003**, in press.

Results

The probability of observing a water pair with separation r and angle θ (defined in Figure 1) is described by a joint radial/angular distribution function $\rho(r,\theta)$, evaluated using computer simulations of water with or without solute present. To describe the effect of solutes on water structure, we start with an analysis of $\rho(r,\theta)$ for pure liquid water (Figure 2a). There are two peaks separated by a saddle point at approximately (3.1 Å, 38°). Projection of $\rho(r,\theta)$ onto the separation axis recovers the familiar radial distribution function, $g(r)$ (inset, Figure 2a), with first and second peaks at 2.8 and 4.5 Å separated by the first minimum at 3.5 Å, positions in close agreement with recent measurements.[12,13] $\rho(r,\theta)$ can be interpreted by comparison with the distribution for ideal tetrahedral ice (ice *Ih*) whose structure is relatively simple (Figure 2b). In ice, the peak at (2.76 Å, 0°) comes from the four hydrogen-bonded (H-bonded) (first coordination shell) neighbors of a water molecule. The second coordination shell of 12 waters H-bonded to the first shell produces three peaks: 10 pairs at (4.5 Å, 35°), 1 at (4.5 Å, 74°), and 1 at (4.5 Å, 90°). It should be noted that in real ice *Ih* these peaks would be broadened in both directions due to thermal motion, slight deviations of the HOH water angle from the ideal tetrahedral angle, and the proton disorder. The ideal ice distribution is presented simply to aid the interpretation of the liquid distributions.

In liquid water, the narrow peak at lower distance/angle is clearly derived from the first coordination shell of ice, but with slightly longer and bent H-bonds due to thermal disorder (mean length/angle of 2.84 Å, 16°). The broader peak at higher angle is formed from the coalescence of peaks in the second and possibly higher coordination shells of ice. Unlike the first shell, though, much of this water moves closer upon melting (hence, the well-known increase in density). At larger separations (>4.0 Å), the angular distribution within the second peak approaches that expected for random orientation (inset, Figure 2b) with a maximum around 40°, indicating the limit of pairwise ordering in liquid water. It should be noted that the random distribution is skewed to lower angles relative to the sine distribution expected for a single randomly oriented OH because the minimum of the four HOO angles is chosen from each configuration.

The observation that the $\rho(r,\theta)$ distribution is bimodal naturally suggests that changes in $\rho(r,\theta)$ can be described in a simple but quantitative fashion by evaluating the relative probability, or equivalently the number of water pairs, in the first peak ($r < 3.1$ Å and $\theta < 38°$), designated N_I, and in the second peak 3.1 Å $< r <$ 4.5 Å or $\theta > 38°$ designated N_{II} (4.5 Å being the position of both the second shell in ideal ice *Ih* and the second maximum in pure water OO $g(r)$). For pure water, $N_I = 3.8 \pm 0.1$ and $N_{II} = 10.1 \pm 0.2$ pairs, respectively, for a total of $N_t = 13.9 \pm 0.3$ pairs within 4.5 Å. The fraction of water pairs $f = N_I/(N_I + N_{II})$ that lie within the first peak, loosely speaking the low angle or "icelike" set, is $3.8/13.9 =$ 27% for pure water, remarkably close to the value of $4/16 =$ 25% for ice *Ih*. Thus, the partial collapse of the open local

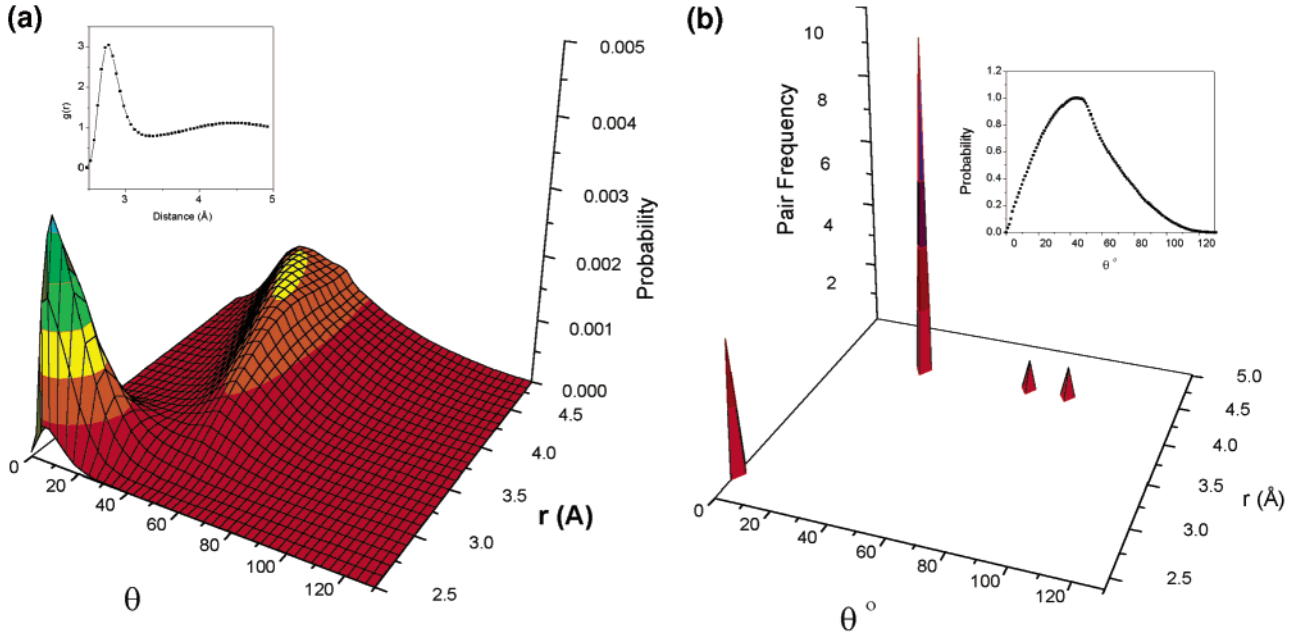

Figure 2. (a) The angle/separation distribution function, $\rho(r,\theta)$, for water pairs in pure liquid water. The vertical axis is the probability of observing a water pair within a 0.1 Å by 1° window. The inset plot shows the standard water O−O $g(r)$ derived from $\rho(r,\theta)$. (b) $\rho(r,\theta)$ for ideal ice *Ih*. Inset: Angle distribution expected for two randomly orientated TIP4P waters evaluated by random sampling.

structure upon melting of water occurs with retention of significant tetrahedral H-bonding structure. A significant portion (1.3 ± 0.1 waters) of the second peak extends below 3.5 Å, the first minimum of the O−O $g(r)$, and so lies within the first coordination shell, producing a coordination number of 5.1 ± 0.2. This "intruding" outer shell water has been discussed in previous work (e.g., refs 17, 39−41). It has significantly more bent H-bonds than the other water at the same separation in the first shell. (Hydrogen bonds with large angular distortion are sometimes described as broken, but because there is no consensus on the angle cutoff, a definition allowing for considerable variation in both distance and angle seems more informative than a binary made/broken definition.) Using the common OH−O definition of the H-bond angle, we determined that this population has a mean angle of about 115°, very close to that observed for interstitial water in a previous analysis of pure water.[17] With the HO−O definition of H-bond angle used here, interestingly, the maximum is quite sharply peaked at 52°, about one-half of the tetrahedral angle. We have previously interpreted this as being due to the intruding, more loosely coordinated water being forced to approach "facially" the loose tetrahedron of the other ~4 waters in the first coordination shell.[24,29]

Scattering experiments provide data on the coordination numbers of liquid water to which we can compare our computed values.[12,13] From the number of waters in the first peak of the experimental O−O $g(r)$, the coordination number is about 5, as compared to the value of 5.1 computed here. In contrast, the first peak of the experimental O−H $g(r)$ contains 3.6 waters. If we assume that this peak contains only the more linear H-bonds because the O−H distance is smaller, there is close agreement with the number of "low angle H-bonds" ($N_I = 3.8$) in Figure 2a.

It is clear from the analysis here that the first coordination shell of water contains two populations with distinct angular structure, a fact that is important in understanding the effect of solutes on water structure. Figure 3a,b shows $\rho(r,\theta)$ for the first hydration shell of the apolar methyl group and the polar hydroxyl group of ethanol. The apolar group depresses the population in the high angle peak relative to the low angle peak at all distances, while the position and width of the low angle "icelike" peak are unchanged. In contrast, around the polar group, the low angle peak is depressed and slightly broadened, and the high angle peak is enhanced. The angular probability distribution for water pairs around the apolar group approaches random at large separation (>4.0 Å), whereas around the polar group the random angular distribution is not attained even at separations >4.5 Å, indicating longer range angular ordering of water structure.

We have simulated the hydration of over two dozen solutes including small ions, denaturants, osmolytes, amino acids, and nucleic acid bases and observe the same general pattern in $\rho(r,\theta)$: There are always two distinct peaks, separated in distance/angle by a saddle point at approximately (3.1 Å, 38°). Solute groups modulate the relative heights of the two peaks one way or the other, depending on whether they are apolar or polar. These effects are confined primarily to water within the first hydration shell. $\rho(r,\theta)$ between first and second shell water pairs shows no dependence on solute polarity and is very similar to that of bulk water (Supporting Information). The $\rho(r,\theta)$ between second shell waters is indistinguishable from bulk water. Analysis of the other four angles that define the mutual orientation of two waters (results available as Supporting Information) shows that, with the exception of the acceptor HO−O angle ψ, the distributions were quite flat and rather insensitive to the presence of polar or apolar solutes. ψ showed distributions very similar to those of θ, but reflected about 50°, with broader distributions and less distinct peaks. Thus, ψ yields

(39) Narten, A.; Levy, H. *J. Chem. Phys.* **1971**, *55*, 2263−9.
(40) Matubayasi, N. *J. Am. Chem. Soc.* **1994**, *116*, 1450−6.
(41) Cho, H.; Singh, S.; Robinson, G. *J. Chem. Phys.* **1997**, *107*, 7979−88.

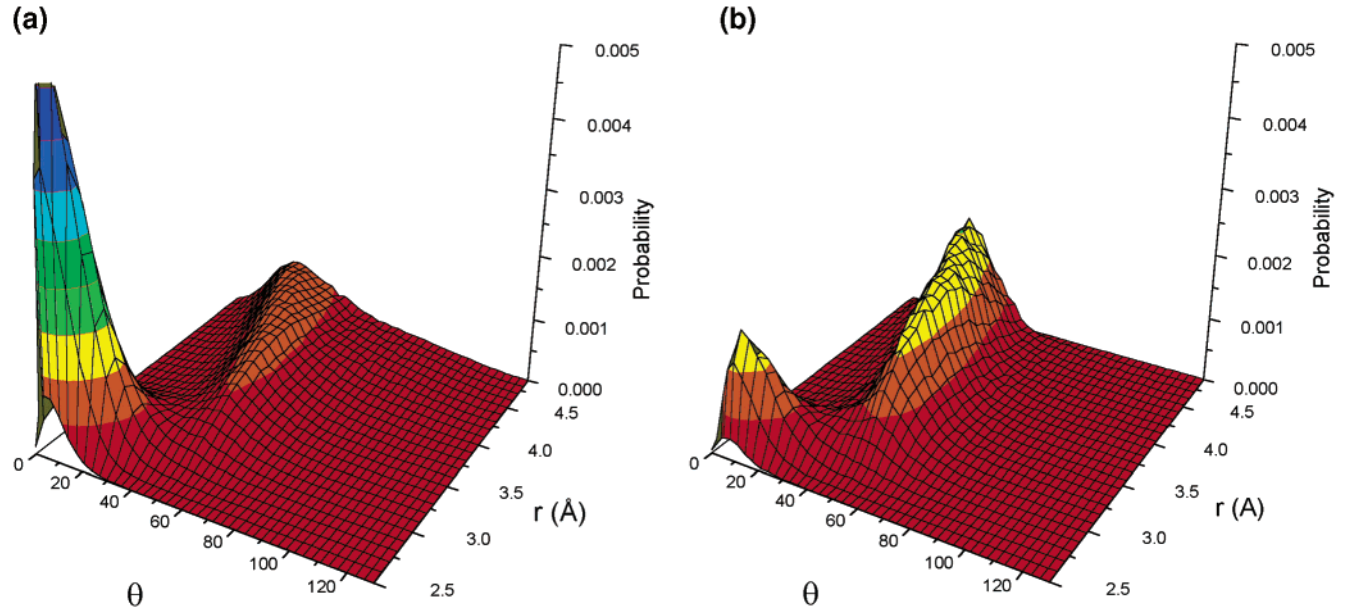

Figure 3. (a) $\rho(r,\theta)$ for water pairs in the first hydration shell of the methyl group of ethanol. (b) $\rho(r,\theta)$ for water pairs in the first hydration shell of the hydroxyl group of ethanol.

the same kind of structural information as θ but at lower resolution, and so it was not analyzed in more detail. This broader distribution of the acceptor angle HO−O angle has been observed in earlier studies of water's orientational structure.[16,17]

The effect of apolar groups can be interpreted primarily in geometric terms: These groups occupy volume but interact weakly with water, so a hydrating water molecule can retain much of its first coordination shell hydrogen bonding geometry with almost no increased distortion, but there is displacement of its more weakly interacting water at larger separation/angle. Polar groups, in contrast, interact with water more strongly, favoring a radial orientation of the water dipole,[22] which causes the increase in population of higher angle water−water geometries seen here, thereby reducing the amount of tetrahedral structure. Although this is clearly less "icelike", whether one would characterize this as "breaking" of water structure is arguable, because the highly nonuniform $\rho(r,\theta)$'s in Figure 3 indicate plenty of structures in both cases, but of a different sort.

To relate these changes to the hydration heat capacities of these solutes, we can define a net excess of low angle geometry or "icelike" pairs relative to high angle pairs within a solute's first hydration shell, as compared to bulk water, as

$$\Delta N = N_t(f - f^{bulk}) \qquad (2)$$

which is the product of two terms: $N_t = N_I + N_{II}$, the total number of water pairs in the first hydration shell of the solute separated by <4.5 Å, and $(f - f^{bulk})$, where f^{bulk} and f are the fractions of low angle pairs (r < 3.1 Å and θ < 38°) in bulk water and in the solute's hydration shell, respectively. f^{bulk} = 27% is the first peak fraction ($N_I/(N_I + N_{II})$) for pure water. Thus, $N_t f^{bulk}$ is the number of low angle pairs expected if the hydration shell structure were the same as that of bulk solvent. ΔN depends on both the size of the first hydration shell through the extensive term N_t and the polarity of each solute atom through the intensive "water structure change" term $(f - f^{bulk})$, and it provides a simple but physically intuitive measure of the distortion in water structure. Positive values of ΔN indicate an excess of low angle/distance relative to high angle/distance water pairs, while negative values indicate a deficit of low angle/distance relative to high angle/distance water pairs. Apolar groups are surrounded by a relative excess of low angle water geometry pairs, while polar groups have a deficit (Table 1), or, equivalently, apolar and polar groups have a relative deficit and excess of high angle/distance pairs, respectively. Moreover, ΔN is highly correlated with the measured ΔC_p for solutes of widely differing hydrophobicity/hydrophilicity (R = 0.97, Figure 4). This is primarily due to the redistribution of the relative low angle/high angle geometry plus the size of the hydration shell, because the correlation of ΔC_p is significantly lower with the "size" of the hydration shell N_t net number of low angle pairs

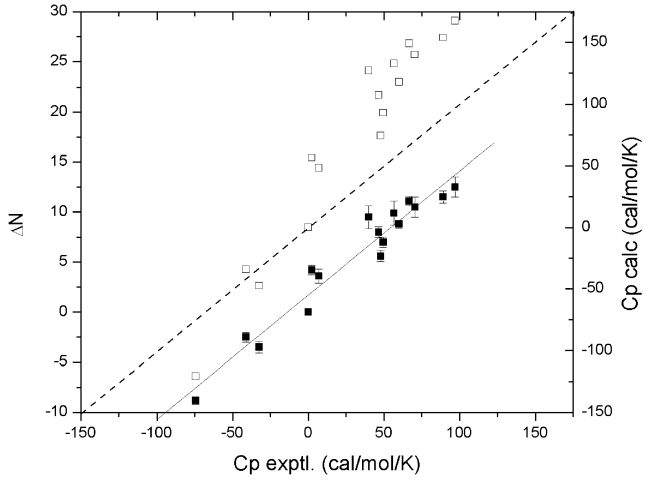

Figure 4. Filled symbols/left ordinate: Excess/deficit low angle geometry water pairs in the first hydration shell, ΔN, versus measured hydration heat capacity, ΔC_p, for solutes listed in Table 1. The solid line is the best linear fit (R^2 = 0.97), excluding the pure water point. Data for salts were taken from Marcus;[9] other solutes were taken from Cabani.[7] Unfilled symbols/right ordinate: Calculated heat capacity using the ΔN from Table 1 and the mean squared energy fluctuation distribution in Figure 5b. The dotted line indicates C_p calc = C_p exptl.

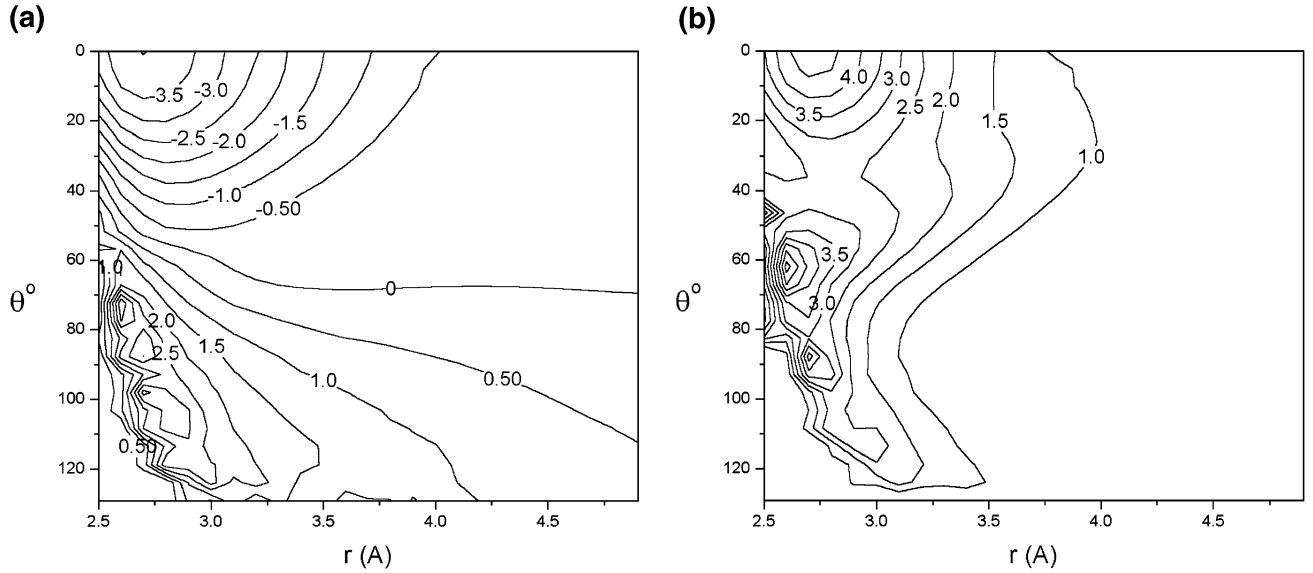

Figure 5. (a) Contour map of the mean water−water pair energy as a function of r and θ. Energies are in kcal/mol/pair. (b) Contour map of the mean squared fluctuation in water−water pair energy as a function of r and θ. Units are in (kcal/mol)^2/pair.

N_{I}, high angle pairs N_{II} (Table 1), or their simple difference ($R = 0.3$).

Given the correlation between ΔC_p and ΔN, if there is a causal relationship between the two, one can infer from the last equality in eq 1 that the energy fluctuation between water pairs (and hence the C_p contribution) must increase with their decreasing angle/separation. To examine this, the mean and mean square fluctuation in water pair energy as a function of r and θ ($\langle E\rangle(r,\theta)$ and $\langle \delta E^2\rangle(r,\theta)$, respectively) were extracted from the simulations. These distributions are shown in Figure 5a,b. For a particular r/θ, the mean pair energy $\langle E\rangle(r,\theta)$ is the average over the configurations sampled by the other four angles describing the pair orientation in the liquid. Similarly, there is a fluctuation in this energy, $\langle \delta E^2\rangle(r,\theta)$, due to configurational fluctuations in these other four angular coordinates, principally from fluctuations in ψ. Figure 5a shows, not surprisingly, that closer water pairs with more linear H−O−O angles have a stronger (more negative) mean interaction energy. Figure 5b shows that closer water pairs with more linear H−O−O angles produce correspondingly larger fluctuations in energy. A priori, it is not obvious that more strongly interacting waters would have larger fluctuations; one could equally expect that the stronger interactions might reduce fluctuations. However, the simulations results in Figure 4 reveal such a correlation between strength of interaction and size of fluctuation. The physical picture of a decrease in water pair distance/angle being accompanied by an increase in C_p is also supported by the form of the C_p equation of state derived from the random network model of water.[14,24,34]

The energy fluctuation map peaks at low distance/angle (ca 2.75 Å/0°) close to the minimum in mean energy, but there is also a second peak at (ca. 2.6 Å/60−80°). The second peak is of little importance, however, because Figures 2 and 3 show that the probability of observing water pairs with configurations in this region is very low. The first peak in the energy fluctuation map, however, occurs in a region that is well populated and undergoes large population shifts in response to solute. The correlation between ΔC_p, ΔN, and pair energy fluctuations is necessary, although not sufficient, for these structural changes to be causally related to the observed hydration heat capacities. To strengthen the argument still further, one can obtain from $\rho(r,\theta)$ and $\langle \delta E^2\rangle(r,\theta)$ an estimate of the average change in mean squared energy fluctuation for a water pair whose geometry shifts from the high angle/distance peak to the low angle/distance peak as follows. Summation of $\rho(r,\theta)\cdot\langle \delta E^2\rangle(r,\theta)$ for $r < 3.1$ Å and $\theta < 38°$ yields the mean squared energy fluctuation for peak I. Summation of $\rho(r,\theta)\cdot\langle \delta E^2\rangle(r,\theta)$ over the remaining r/θ space yields the corresponding value for peak II. The difference gives $\Delta C_p{}^{\mathrm{calc}}/\Delta N = 13.9$ cal/mol/K/water pair. This value can be used to convert the solute ΔN values to estimates of ΔC_p. The results are plotted in Figure 4 and tend to overestimate the measured values by about 50%. A modest overestimate like this may well be explained by neglect of correlations between water pair fluctuations in our analysis, and with solute−water fluctuations. Such correlations would have the effect of reducing the total energy fluctuation. Nevertheless, the excellent correlation between the calculated and measured ΔC_p values ($R = 0.97$), plus the fact that the computed energy fluctuations have the right size to explain the data, strongly implicate the first hydration shell structure changes described here as the primary origin of the hydration heat capacity effects.

Two of the solutes in Table 1 are of additional interest beyond their C_p effects because of their effect on protein stability: Urea is a strong protein denaturant, and trimethylamine oxide (TMAO) is one of the most potent protein stabilizers (osmolytes). It has been suggested that urea acts through its "structure breaking" effect on water, weakening the hydrophobic effect. Although urea and TMAO have opposite effects on protein stability, their $\rho(r,\theta)$ distributions are very similar and not dramatically different from that of pure water (Figure 6). This supports a direct mode of action involving favorable and unfavorable interactions, respectively, with the peptide groups,[42,43] rather than indirectly by modulating water structure. The lack of either significant breaking or formation of water structure by urea is consistent with recent spectroscopic measurements showing little effect of this solute.[32]

(42) Bolen, D. W. *Biophys. J.* **1998**, *74*, A219.
(43) Wang, A. J.; Bolen, D. W. *Biophys. J.* **1996**, *70*, SuAM7.

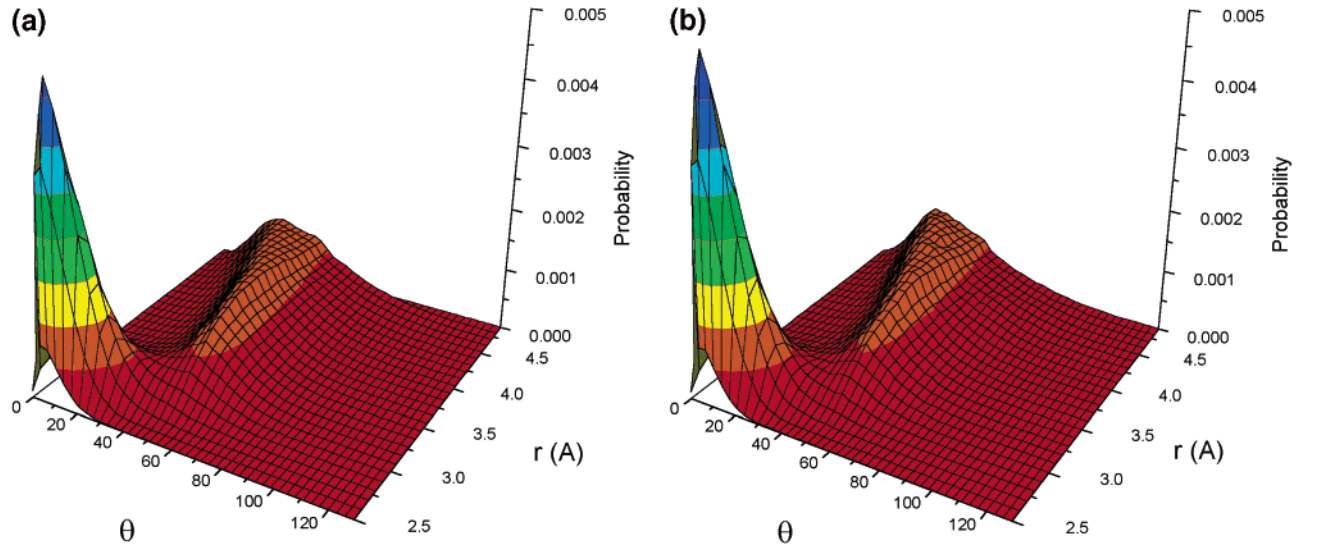

Figure 6. (a) $\rho(r,\theta)$ for water pairs within the first hydration shell of urea. (b) $\rho(r,\theta)$ for water pairs within the first hydration shell of TMAO.

Discussion

The description of water structure presented here is based on the analysis of water pair configurations in terms of two principal coordinates: the O−O separation and the HO−O "donor" angle. The results may be summarized as follows. Two predominant water pair geometries are seen in pure water: a low angle/separation pair derived from the first coordination shell of ice and a higher angle configuration with a more varied separation ranging between first and second coordination shells. The primary effect of solutes is to alter the relative populations of these two configurations in their first hydration shell: Apolar solutes and groups increase the low angle/separation pair population, while polar solutes/groups increase the high angle population. The effect of apolar solutes is primarily geometric: While occupying volume, they interact with water weakly and so displace the high angle/separation "weaker" coordinated water, favoring low angle/separation "strongly" coordinated water geometries. Polar groups tend to orient water dipoles radially through stronger electrostatic interactions, which distorts the water−water configurations to high "H-bond" angles. Augmentation of "stronger" more linear H-bonds around apolar groups has been well documented in simulations.[21,22,44−48] Here, we relate this augmentation, and the complementary diminishment of such H-bonds around polar groups, to their effect on hydration heat capacity. Low angle/separation water pair configurations have stronger interactions, and it turns out that this, combined with structural fluctuations, leads to larger energy fluctuations. Thus, the relative increase in the low angle/separation population around apolar groups results in an increase in heat capacity, while the decrease in their population around polar groups results in a decrease in heat capacity. These changes in population are highly correlated with the experimental heat capacity changes for a wide range of solute sizes, polarity, and shape and involve energy fluctuations of about the right size, strongly implying that these are the causative structural effects with regard to hydration C_p.

The structural effects we see are confined primarily to the first hydration shell, which is consistent with the prevailing view, based on group additivity and area proportionality arguments, that hydration C_p effects arise primarily from first hydration shell effects.[49−55] While our analysis of the water structure was not confined a priori to the first hydration shell, nor did it assume a "two-state" H-bond model, these features emerged naturally from the simulation results. Previous work on the hydration enthalpy and entropy of apolar solutes[48,56,57] provides several key supports for hydration shell type models. First, about 70% of the hydration enthalpy of apolar solutes can be accounted for by the first hydration shell. Second, excess partial molar enthalpies and entropies of apolar solutes can be expressed accurately in terms of local components. Third, this work provides a picture of the enthalpy/entropy balance in solvation, which also shows an increase in H-bonding strength in the first hydration shell. The strong correlation between hydration C_p changes and first hydration shell structure described here suggests that these hydration shell concepts extend also to heat capacity effects, and to both polar and apolar solutes.

Thermodynamic data and theoretical considerations indicate that there is a size dependence on the hydrophobic effect.[19,58] For larger hydrophobic surfaces, the unfavorable free energy is larger on a unit area basis and becomes (at room temperature) enthalpically driven, rather than entropically driven. It has been suggested that the origin of the hydrophobic effect is different at larger length scales operating in protein folding, occurring

(44) Rossky, P. J.; Karplus, M. *J. Am. Chem. Soc.* **1978**, *100*, 1913.
(45) Pangali, C.; Rao, M.; Berne, B. J. *J. Chem. Phys.* **1979**, *71*, 2982−90.
(46) Geiger, A.; Rahman, A.; Stillinger, F. H. *J. Chem. Phys.* **1979**, *70*, 263−76.
(47) Rossky, P. J.; Zichi, D. A. *Faraday Symp. Chem. Soc.* **1982**, *17*, 69.
(48) Gallicchio, E.; Kubo, M.; Levy, R. M. *J. Phys. Chem. B* **2000**, *104*, 6271−85.
(49) Murphy, K.; Gill, S. *Thermochim. Acta* **1990**, *172*, 11−20.
(50) Murphy, K. P.; Gill, S. J. *J. Mol. Biol.* **1991**, *222*, 699−709.
(51) Robertson, A. D.; Murphy, K. P. *Chem. Rev.* **1997**, *97*, 1251−67.
(52) Makhatadze, G.; Privalov, P. *J. Mol. Biol.* **1990**, *213*, 385−391.
(53) Makhatadze, G.; Privalov, P. *J. Mol. Biol.* **1990**, *213*, 375−384.
(54) Livingstone, J. R.; Spolar, R. S.; Record, T. M. *Biochemistry* **1991**, *30*, 4237−4244.
(55) Spolar, R.; Livingstone, J.; Record, M. T. *Biochemistry* **1992**, *31*, 1, 3947−55.
(56) Matubayashi, N.; Reed, L.; Levy, R. M. *J. Phys. Chem.* **1994**, *98*, 8, 10640−9.
(57) Matubayasi, N.; Gallicchio, E.; Levy, R. M. *J. Chem. Phys.* **1998**, *109*, 4864−72.
(58) Sharp, K. A.; Nicholls, A.; Fine, R. M.; Honig, B. *Science* **1991**, *252*, 106−109.

with weakening rather than strengthening of water−water interactions.[19,59] While this study examined solutes varying over about a 6-fold size range, the largest are still small as compared to a protein. It is therefore of interest to consider if such size effects would invalidate the applicability of the results presented here to protein folding, and hence to the explanation of cold denaturation of proteins. There are several arguments to the contrary. First, the total C_p change for protein unfolding is well approximated by the sum of the individual contributions of its constituents, as was measured on solutes of comparable size to those in Table 1.[52,53] Second, these putative size effects have only been demonstrated for purely apolar spherical solutes of increasing radius. A protein surface consists of a mosaic of polar and apolar regions of varying curvature, whose local polarity/topology closely resembles the small solute analogues of amino acids or fragments, that is, backbone/NMA, phenylalanine/benzene, etc. Third, the increase in heat capacity upon protein unfolding results from the exposure of previously buried groups which are now hydrated in the unfolded state, that is, in a state with local curvature/topology similar to that of its constituent groups. Thus, given that the phenomenon of cold denaturation of proteins arises from the net positive heat capacity change upon unfolding, and that this is attributable to the additive effects of the constituent groups, an explanation for the hydration C_p of small solutes proposed here would satisfactorily account for the cold denaturation effect.

It should also be noted that hydration of apolar groups is accompanied by decreases in both enthalpy and volume,[1,7] which can also be accounted for by an increase in the population of low angle/separation water pairs in the first hydration shell described here. Because the enthalpy and volume changes have significant contributions in addition to first hydration shell water−water effects, further quantitation of these relations using the approach described here will be pursued in a future study.

Several other mechanisms for the increase in water C_p around apolar groups have been proposed. Lee,[60] using scaled particle theory, has attributed it to the small size of water and the entropy necessary to create a cavity for the solute. Garde et al., using pure water simulations analyzed using information theory, explain the C_p increase in terms of the small temperature dependence of the isothermal compressibility of water. In this study and an earlier model for hydrophobicity[61] which also predicts a positive apolar hydration C_p, the key element is Gaussian type fluctuations in water that create cavities for apolar solutes. Chandler[59] has attributed the increased apolar solubility upon lowering the temperature, responsible for cold denaturation of proteins, to the effect of temperature in moving the hydrating water away from its liquid−vapor water transition. Although different causative effects are proposed in each of these models, the common feature is that they are all based on a description of water in terms of its radial distribution functions. Thus, the orientational effects of water appear only implicitly.[19] Whether the reasons for the C_p changes described by these models can be reconciled, and whether they reflect the effect of explicit angular changes in water structure of the kind described here, or alternative structural effects, remains to be seen. In addition, these models have to date only been developed for treating spherical purely apolar solutes (i.e., spherical cavities or hard sphere solutes). So, whether they can account for the decrease in C_p around polar groups, and Cp changes caused by solutes of varied shape and mixed polarity, also remains to be seen. Direct comparison with these models at this point is thus difficult. Any satisfactory structural explanation for the hydration C_p effects must, however, encompass both apolar and polar groups within the same physical framework and must apply to solutes of varied shape, size, and heterogeneous polarity.

In summary, the analysis of angular water structure presented here provides new insights into the differential hydration of apolar and polar groups and a plausible structural and quantitative explanation of heat capacity changes, a "signature" of the hydrophobic effect.

Acknowledgment. This work was supported by grant GM 54105 from the NIH.

Supporting Information Available: Plots of the secondary water−water orientation angles ψ, ϕ, χ, and ω for $r = 2.8$, 3.5, and 4.4 Å for pure water, and first−first shell water pairs around argon and K^+ and $\rho(r,\theta)$ plots for first−second shell water pairs around argon and K^+ (PDF). This material is available free of charge via the Internet at http://pubs.acs.org.

JA029796N

(59) Chandler, D. *Nature* **2002**, *417*, 491.
(60) Lee, B. *Biophys. Chem.* **1994**, *51*, 271−7.
(61) Pratt, L.; Chandler, D. *J. Chem. Phys.* **1977**, *67*, 3683−3705.